2

ORNL/Sub/88-07685CT92/01

AQUEOUS CORROSION CHARACTERISTICS AND CORROSION-RELATED CRACKING SUSCEPTIBILITIES OF Fe_3Al-TYPE IRON ALUMINIDES

April 1991

Report Prepared by

R. A. Buchanan and J. G. Kim
Department of Materials Science and Engineering
The University of Tennessee
Knoxville, TN 37996-2200

under
Subcontract Number 41B-07685C T92

for

OAK RIDGE NATIONAL LABORATORY
Oak Ridge, Tennessee 37831

managed by
MARTIN MARIETTA ENERGY SYSTEMS, INC.
for the
U.S. Department of Energy
under Contract No. DE-AC05-84OR21400

ORNL/Sub--88-07685/01

DE91 013028

AQUEOUS CORROSION CHARACTERISTICS AND CORROSION-RELATED CRACKING SUSCEPTIBILITIES OF Fe_3Al-TYPE IRON ALUMINIDES

April, 1991

Research sponsored by the U. S. Department of Energy,
Fossil Energy
Advanced Research and Technology Development Materials Program

Report Prepared by

R. A. Buchanan and J. G. Kim
Department of Materials Science and Engineering
The University of Tennessee
Knoxville, TN 37996-2200

under
Subcontract Number 41B-07685C T92

for

OAK RIDGE NATIONAL LABORATORY
Oak Ridge, Tennessee 37831
managed by
MARTIN MARIETTA ENERGY SYSTEMS, INC.
for the
U.S. Department of Energy
under Contract No. DE-AC05-84OR21400

CONTENTS

LIST OF TABLES iv

LIST OF FIGURES v

INTRODUCTION 1

PROCEDURES AND RESULTS 2

POLARIZATION TESTS AND CORROSION RATE MEASUREMENTS 2

IMMERSION TEST RESULTS 20

U-BEND CORROSION CRACKING TESTS 21

SLOW-STRAIN-RATE CORROSION TESTS 27

SUMMARY AND CONCLUSIONS 30

REFERENCES 34

APPENDIX: DISTRIBUTION LIST 37

LIST OF TABLES

Table 1. Results of electrochemical evaluations of average corrosion penetration rates 5

Table 2. Results of 200h mass-loss immersion tests, converted to average corrosion penetration rates 6

Table 3. Compositions of selected iron aluminides (at. %)..... 13

Table 4. Corrosion rates by the polarization-resistance method..... 15

Table 5. Chemical compositions of iron aluminides..... 17

Table 6. Electrochemical corrosion characteristics in aerated synthetic seawater 19

Table 7. Average penetration rates by polarization-resistance measurements in aerated 1N sulfuric acid..... 20

Table 8. Immersion test results, acid-chloride solution, visual-corrosion-product initiation times 21

Table 9. U-bend results at open-circuit corrosion potentials (E_{corr}) 22

Table 10. U-bend test results in acid-chloride solution over a range of applied potentials..... 25

Table 11. Slow-strain-rate corrosion test results 29

LIST OF FIGURES

Fig. 1 Typical cyclic anodic polarization behavior of iron aluminides 3

Fig. 2 Cyclic anodic polarization behavior of nickel-iron aluminide 5

Fig. 3 Cyclic anodic polarization behavior of annealed iron aluminides in aqueous solution containing 200 ppm Cl^- at pH = 4 7

Fig. 4 Cyclic anodic polarization behavior of cold-worked iron aluminides in aqueous solution containing 200 ppm Cl^- at pH = 4 8

Fig. 5 Cyclic anodic polarization behavior of stainless steels, nickel-iron aluminide, and iron aluminide (6% Cr) 9

Fig. 6 Effects of Mo on the cyclic anodic polarization behavior of 2% Cr iron aluminide 10

Fig. 7 Effects of Mo on the cyclic anodic polarization behavior of 4% Cr iron aluminide 10

Fig. 8 Iron-aluminum phase diagram 11

Fig. 9 Effects of structure on anodic polarization behavior 12

Fig. 10 Cyclic anodic polarization behavior in acid-chloride solution 14

Fig. 11 Anodic polarization behavior in thiosulfate solution 14

Fig. 12 Anodic polarization behavior in tetrathionate solution 15

Fig. 13 Effects of Cr and Nb on cyclic anodic polarization behavior 16

Fig. 14 Cyclic anodic polarization behavior in aerated, pH = 4, 200 ppm Cl^- solution 17

Fig. 15 Cyclic anodic polarization behavior in aerated synthetic seawater 18

Fig. 16 Cyclic anodic polarization behavior in aerated 1N sulfuric acid 19

Fig. 17 Anodic and cathodic polarization curves for FA-129 iron aluminide in acid-chloride solution. Applied anodic and cathodic potentials are identified by dashed lines 24

Fig. 18 Tensile specimen geometry employed at ORNL, with slow-strain-rate-corrosion fracture locations identified 27

Fig. 19 Current slow-strain-rate corrosion test-specimen geometry 29

AQUEOUS CORROSION CHARACTERISTICS AND CORROSION-RELATED CRACKING SUSCEPTIBILITIESOF Fe_3Al-TYPE IRON ALUMINIDES*

R. A. Buchanan and J. G. Kim

INTRODUCTION

Fe3Al-type iron aluminides have been shown to exhibit excellent high-temperature oxidation properties at relatively low cost, making them exceptional candidates for fossil-energy applications.[1,2] However, in past years these materials have been characterized by very low room-temperature ductilities (3-5%).[3-6] Recently, efforts have been devoted to improving the ductilities through control of grain structure, alloy additions and material processing.[7-16] Studies at the Oak Ridge National Laboratory (ORNL) have shown that the room-temperature ductility can be significantly improved by additions of up to 6% Cr.[17-19] Mechanisms responsible for this beneficial effect have been elucidated.[17-23]

In certain fossil-energy applications, the iron aluminides may also be subjected to ambient-temperature aqueous corrosion conditions. In the present project, the aqueous corrosion characteristics and the cracking tendencies under aqueous-corrosion conditions were studied. In these studies, electrochemical, immersion and electrochemical-mechanical evaluation techniques were employed.

For a range of iron-aluminide compositions, cyclic anodic polarization tests were conducted in a number of electrolytes to provide information on anodic dissolution characteristics including tendencies for either active uniform corrosion, localized corrosion, or passivation. Average corrosion penetration rates were determined by application of Tafel methods or the polarization-resistance method in combination with Faraday's law. Immersion test methods were employed to verify corrosion behavior as determined by electrochemical methods and to evaluate localized-corrosion initiation times. U-bend corrosion tests were conducted at open-circuit corrosion potentials and at potentiostatically-controlled anodic and cathodic potentials to investigate the cracking tendencies of selected iron aluminides and to provide information on the cracking mechanism. And finally, slow-strain-rate corrosion tests were conducted at open-circuit and potentiostatically-controlled cathodic potentials to study the ductility response as related to cracking tendencies and the mechanism responsible.

*Research sponsored by the U.S. Department of Energy, Fossil Energy AR&TD Materials Program, DOE/FE AA 15 10 10 0, Work Breakdown Structure Element UTN-3

PROCEDURES AND RESULTS

Polarization Tests and Corrosion Rate Measurements

Initially in the project, the objectives involved corrosion characterizations of four iron-aluminide compositions and one nickel-iron aluminide. All materials were fabricated at ORNL. The nominal compositions (atomic percent (at. %)) of these iron aluminides were Fe-28Al, Fe-28Al-2Cr, Fe-28Al-4Cr, and Fe-28Al-6Cr, with designations of FA-61, FA-77B, FA-72C, and FA-78, respectively. These alloys were evaluated in both air-annealed (1 h at 850°C plus 2d at 500°C) and 10% cold-worked conditions. The nickel-iron aluminide (70.66% Ni, 11.2% Fe, 9.54% Al, 6.95% Cr, 0.35% Zr, 1.28% Mo, 0.02% B), designated as alloy 357, was evaluated in the vacuum-annealed condition (1h at 1100°C).

All samples for electrochemical evaluations were prepared in the following manner. An electrical connection was made to each specimen by means of a soldered brass screw on the back sample surface. The sample was then mounted in Maraglas 655 epoxy, and the front sample surface was uniformly exposed by wet grinding with 600 grit SiC paper. The metal/epoxy interface was coated with Glyptal 1201 Red Enamel to minimize problems with interface crevice corrosion. The exposed metal surface was again ground with 600 grit SiC paper to remove air-formed oxide films immediately before attachment of the mounted sample to a glass-insulated sample holder and immersion into the electrolyte of the polarization cell.

The program initially involved anodic polarization testing at ambient laboratory temperature in four electrolytes over a wide pH range: 1N HCl (pH ~ 0.5), 1N H_2SO_4 (pH ~ 0.5), 3.5% NaCl (pH = 7), and 1N NaOH (pH ~ 14). This selection of electrolytes also provided indications of the effects of chlorides on corrosion behavior. The electrolytes were continuously saturated with oxygen before and during polarization testing. Each cyclic anodic polarization test consisted of first allowing the steady-state open-circuit corrosion potential to be established (< 1 mV change per minute), then scanning the potential in the anodic direction at a rate of 600 mV/h while measuring the current density. The scanning direction was reversed to complete the cyclic curve at a

terminating current density of 10^{-3} A/cm^2. The results for the initial four iron aluminides (0,2,4, and 6% Cr) and the nickel-iron aluminide are summarized in the following sections.

1N Hydrochloric Acid. This strong hydrochloric acid solution was very aggressive toward the iron aluminides and the nickel-iron aluminide. Only active behavior, i.e. continuously increasing current density with increasing potential, was demonstrated for all materials in all conditions. Examples of this behavior are shown in Figures 1 and 2.

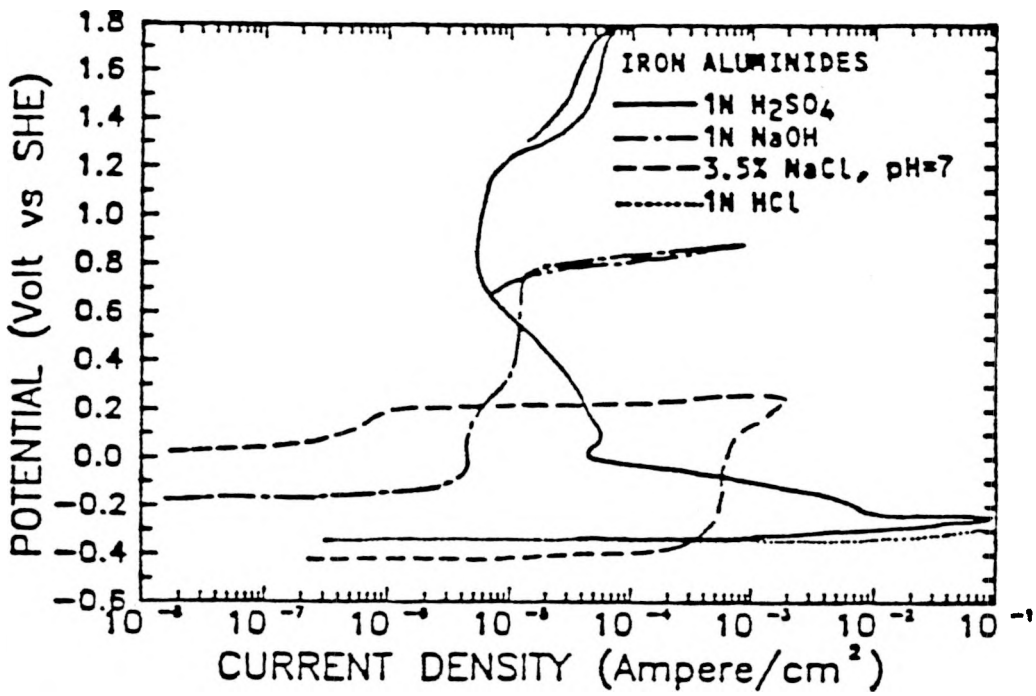

Fig. 1. Typical Cyclic Anodic Polarization Behavior of Iron Aluminides

1N Sulfuric Acid. During the initial series of tests on the iron aluminides, the potential scan direction was reversed at 10^{-1} A/cm^2 after only active behavior was demonstrated in this strong sulfuric acid solution. Subsequent tests indicated that passivation does occur at higher potentials after a critical anodic current density equal to or greater than 10^{-1} A/cm^2 is exceeded. An example is shown in Figure 1. Nevertheless, the corrosion potential for all the iron aluminides in both annealed and cold-worked conditions existed within the active range. The nickel-iron aluminide demonstrated better passivation behavior with a maximum active current density of 10^{-3} A/cm^2 and a passive current density of 10^{-4} A/cm^2.

3.5% NaCl, pH = 7. All materials exhibited passive behavior with hysteresis (a loop within the cyclic anodic curve) in the neutral 3.5% NaCl solution, indicating susceptibility to localized pitting/crevice corrosion. For all of the iron aluminides in both conditions, the protection potential (the potential at which the down-scan current density either equals the up-scan passive current density or its extrapolation to lower potentials) was below the open-circuit corrosion potential (the starting potential for the anodic curve), indicating that localized corrosion could occur during the freely-corroding condition. An example is shown in Figure 1. For the nickel-iron aluminide, the protection potential was above the open-circuit corrosion potential (Figure 2), indicating a higher degree of resistance to crevice/pitting corrosion.

1N Sodium Hydroxide. All materials in all conditions exhibited ideal passive behavior in this very basic solution. Passive current densities were in the 10^{-5} - 10^{-6} A/cm^2 range. Breakdown potentials were quite high, and no hysteresis was exhibited indicating excellent resistance to localized corrosion. An example is shown in Figure 1.

Selected combinations of materials and electrolytes were subjected to electrochemical tests to evaluate corrosion rates under freely- corroding conditions as an additional means to confirm the trends indicated by the previous anodic polarization results. Corrosion rates for the 0% Cr and 6% Cr iron aluminides, and the nickel-iron aluminide, were evaluated. Two methods were employed. The first method involved Tafel extrapolation of cathodic polarization curves to determine corrosion current densities. This method proved difficult in certain cases, however, due to complications arising from nonlinearities in the cathodic curves in the aerated acid solutions. Consequently, a second method, the Tafel statistical method, which was judged to be more accurate, was employed. This method involved small-potential sweeps through the corrosion potential (±25mV) with subsequent statistical analyses. Using the Butler-Volmer model, linear regression was used to obtain first approximations to the Tafel slopes, then nonlinear regression was employed to determine the Tafel slopes and corrosion current density which best fit the experimental data. Once the corrosion current densities were determined, Faraday's law was used to calculate average corrosion penetration rates in mils per year (mpy). Results are presented in Table 1. These results were consistent with indications derived from the polarization behavior of the iron aluminides, that is, relatively high corrosion rates in the strong acids, low average rates in neutral chloride solution (but definite susceptibility to localized corrosion), low rates in the basic solution, and little differentiation of Cr alloying effects.

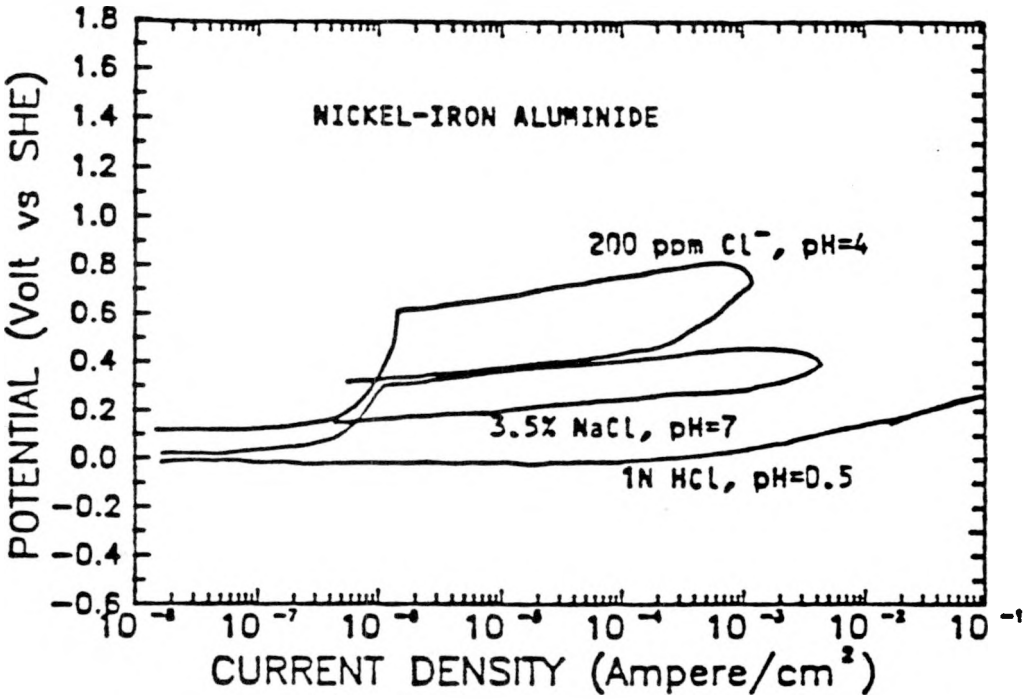

Fig. 2. Cyclic Anodic Polarization Behavior of Nickel-Iron Aluminide

Table 1. Results of Electrochemical Evaluations of Average Corrosion Penetration Rates

Solution	Average Penetration Rate (mpy) by Tafel Statistical Method		
	Fe-28a/o Al (Cold-Worked)	Fe-28 a/o Al + 6 a/o Cr (Cold-Worked)	Nickel-Iron Aluminide (Annealed)
1N HCL	260	255	40
1N H_2SO_4	1460	520	34
3.5% NaCl pH = 7.0	5	0.07	0.20
1N NaOH	0.30	0.10	0.01

Selected materials were also subjected to 200-hour mass-loss immersion tests in selected electrolytes. The mass losses were converted to average corrosion penetration rates (mpy), as given in Table 2. Again, these results were consistent with trends indicated by previous tests.

Table 2. Results of 200h Mass-Loss Immersion Tests, Converted to Average Corrosion Penetration Rates

Solution	Average Penetration Rate (mpy) from Mass-Loss Immersion Tests		
	Fe-28a/o Al (Cold-Worked)	Fe-28 a/o Al + 6 a/o Cr (Cold-Worked)	Nickel-Iron Aluminide (Annealed)
1N H_2SO_4	1710	>2110*	14
3.5% NaCl pH = 7.0	3.8	2.6	0.80

*Total dissolution of sample in 48h.

Based on the above results, and relative to the iron aluminides, it was tentatively concluded that the four electrolytes were either too aggressive (1N HCl, 1N H_2SO_4, and 3.5% NaCl(with respect to localized corrosion)) or insufficiently aggressive (1N NaOH) to allow differentiation of the Cr alloying effects. Consequently, a fifth electrolyte was designed to simulate an aggressive acid-rain-type atmospheric-corrosion situation. This electrolyte consisted of an aqueous solution containing 200 ppm Cl^- (NaCl) at pH = 4 (H_2SO_4). Cyclic anodic polarization and immersion tests were conducted in this solution.

200 ppm chloride, pH = 4. In this solution, the anodic polarization behavior of the nickel-iron aluminide improved relative to the 3.5% NaCl solution by demonstrating higher breakdown and protection potentials (Figure 2), as expected because of the reduced chloride concentration. The average corrosion penetration rate (Tafel statistical method) was found to be 0.10 mpy. For the iron aluminides (Figures 3 and 4), again, the protection potentials were below the corrosion potentials. However, the breakdown potential increased with Cr content, indicating increased relative resistance to initiation of

localized corrosion. Some differences were noted between the annealed (Figure 3) and cold-worked (Figure 4) materials. Generally, for the 2,4, and 6% Cr materials, the cold-working process led to somewhat higher passive current densities and lower breakdown potentials. The 0% Cr iron aluminide did not undergo passivation at all in the cold-worked condition. Average corrosion rates were evaluated by the Tafel statistical method for the cold-worked 0% Cr and 6% Cr iron aluminides. The values were found to be 4.5 and 0.10 mpy, respectively.

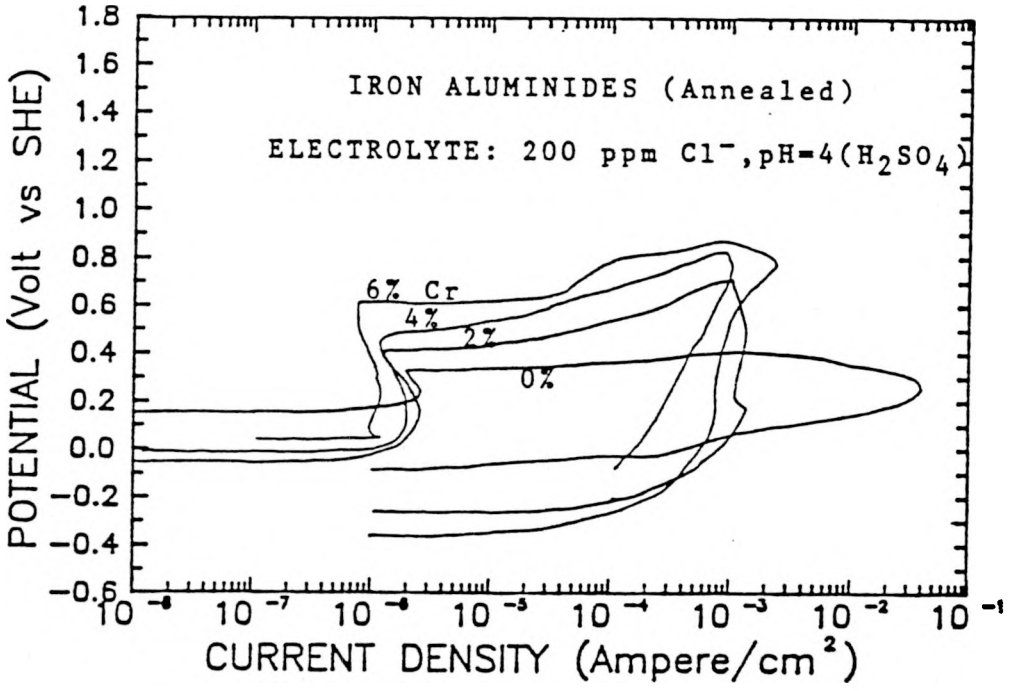

Fig. 3. Cyclic Anodic Polarization Behavior of Annealed Iron Aluminides in Aqueous Solution Containing 200 ppm Cl^- at pH = 4

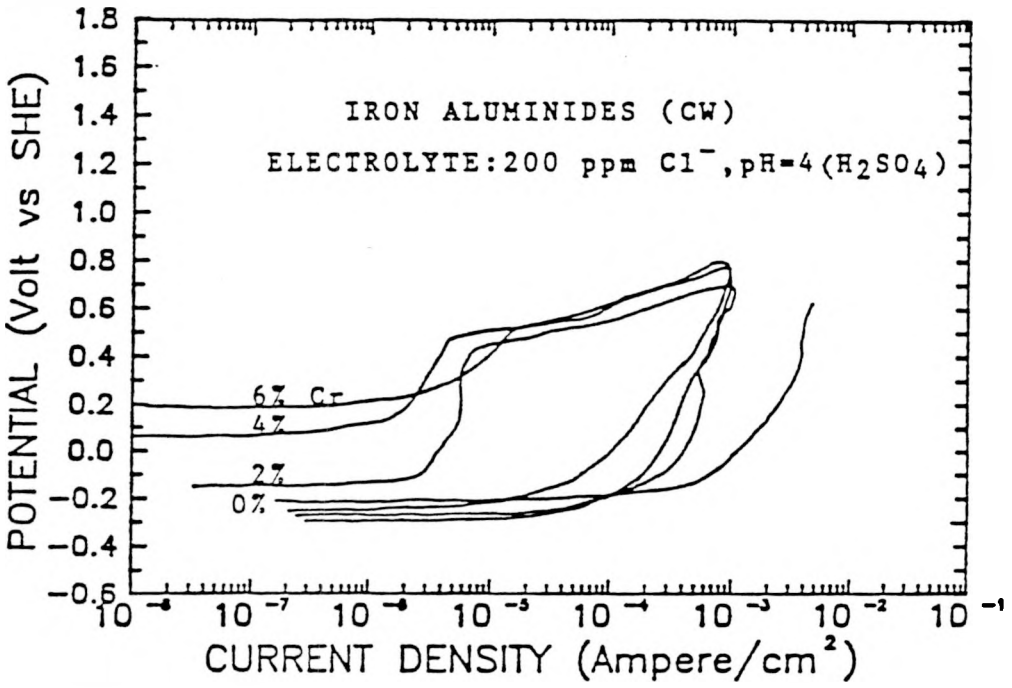

Fig. 4. Cyclic Anodic Polarization Behavior of Cold-Worked Iron Aluminides in Aqueous Solution Containing 200 ppm Cl^- at pH = 4

To provide a frame of reference for comparison, the anodic polarization curves of Types 304L and 316L stainless steel were also determined in the 200 ppm Cl^-, pH=4, electrolyte. These curves along with those of the nickel-iron aluminide and the 6% Cr iron aluminide are compared in Figure 5. It is seen that the major problem associated with the 6% Cr iron aluminide is its low protection potential.

At this point in the evolution of the project, it was recommended to ORNL investigators that iron-aluminide compositions containing Mo, as well as Cr, be evaluated. It was anticipated that Mo additions could improve the resistance to localized corrosion. For this purpose, ORNL supplied two additional air-annealed alloys (1h at 850°C plus 2d at 500°C), both containing 2 at. % Cr, one containing 1 at. % Mo (FA-86), the other 2 at. % Mo (FA-85). The anodic polarization curves for these additional materials, along with that of the 2% Cr iron aluminide containing no Mo (FA-61), are shown in Figure 6. It is apparent from these data that Mo additions raise the protection potential -- an important

result in terms of increasing the resistance of iron aluminides to localized, chloride-induced, aqueous corrosion.

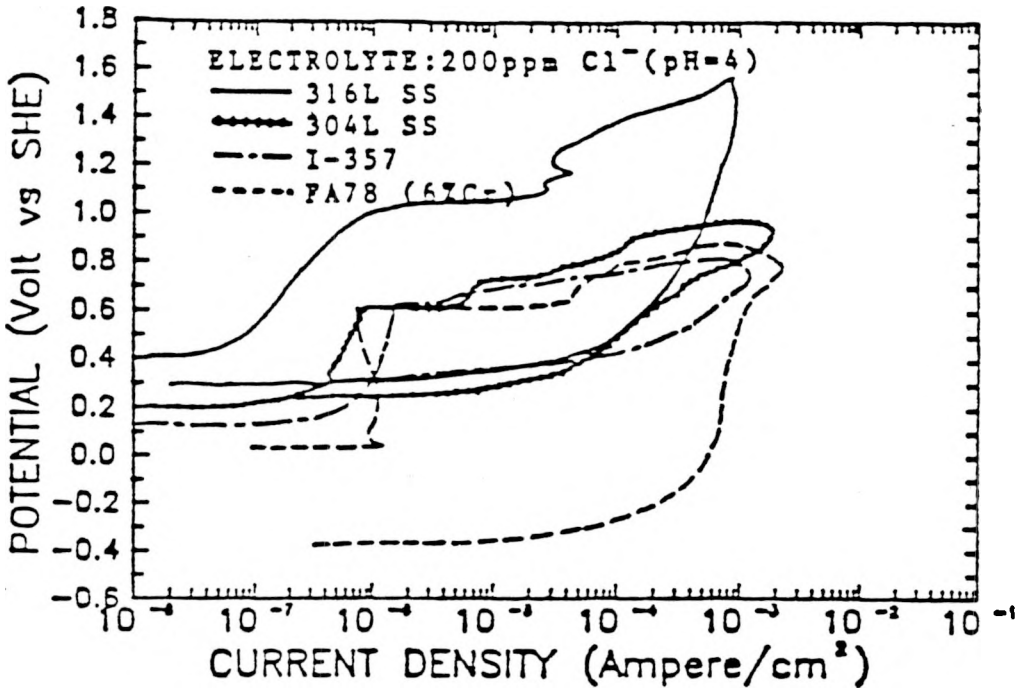

Fig. 5. Cyclic Anodic Polarization Behavior of Stainless Steels, Nickel-Iron Aluminide, and Iron Aluminide (6% Cr)

In view of these promising results, additional air-annealed alloys containing a higher 4 at.% Cr level with 0.5, 1.0, and 2.0 at.% Mo additions were produced by ORNL for corrosion studies. Cyclic anodic polarization tests were conducted in the 200 ppm Cl^-, pH = 4 solution, with the results presented in Figure 7. The polarization characteristics improved relative to the 2% Cr materials (Figure 6). The best response occurred with the 4% Cr + 2% Mo material (FA-140), where as shown in Figure 7, the protection potential was found to be approximately 0.1V above the open-circuit corrosion potential. This was the first iron-aluminide to demonstrate such a favorable polarization response.

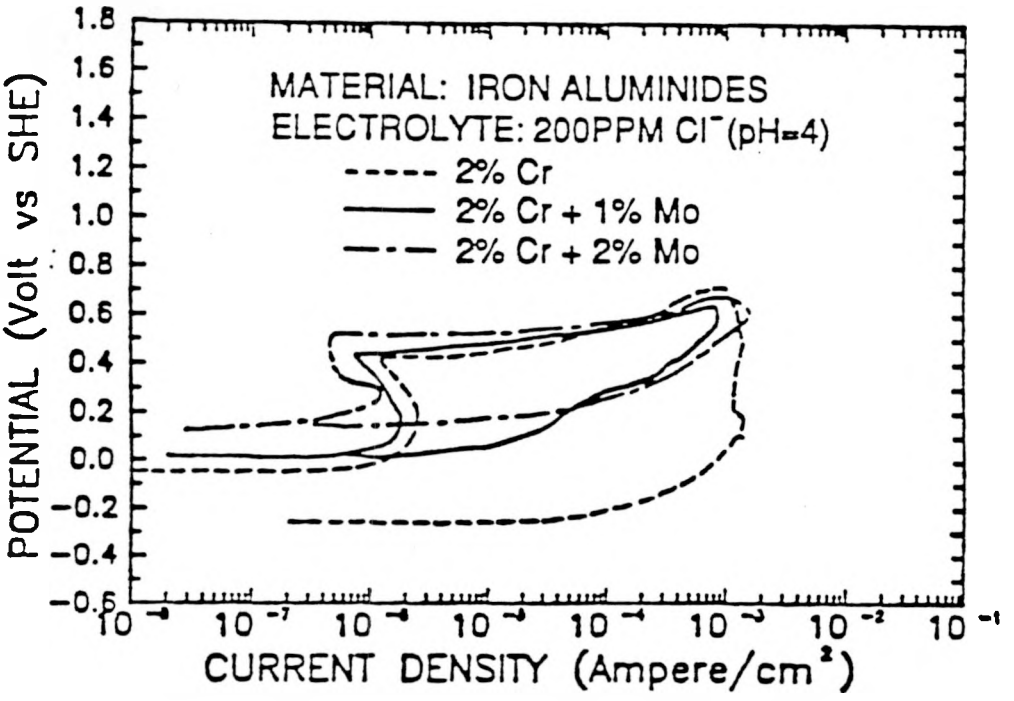

Fig. 6. Effects of Mo on the Cyclic Anodic Polarization Behavior of 2% Cr Iron Aluminide

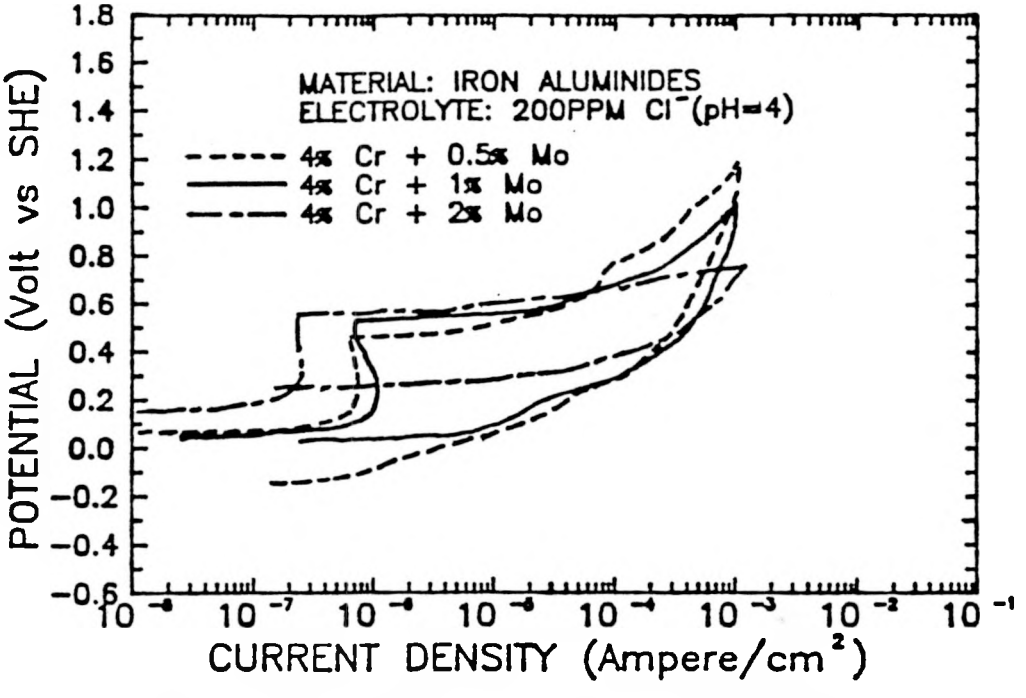

Fig. 7. Effects of Mo on the Cyclic Anodic Polarization Behavior of 4% Cr Iron Aluminide

For the previous materials, ORNL investigators had utilized the following final heat-treatment sequence: 1 hour at 850°C (recrystallization), 2 days at 500°C (ordering heat treatment), then air cooling. With reference to the phase diagram presented in Figure 8, this treatment resulted in the DO_3 superlattice. However, because of improved room-temperature ductility (% elongation via tensile tests), the investigators changed the standard final heat treatment to 1 hour at 750°C followed by an oil quench. This treatment is believed to result in the B2 superlattice at room temperature. It was of interest to evaluate the effect of the change-in-structure (DO_3 vs B2) on corrosion behavior. Samples of FA-140 (Fe-28Al-4Cr-2Mo) were given the two different heat treatments and submitted to cyclic anodic polarization and polarization-resistance testing (600 mV/h scan rate). The polarization curves are compared in Figure 9. The former heat treatment (DO_3 structure) produced somewhat better results: a lower passive current density and a slightly higher localized-corrosion breakdown potential. The polarization-resistance tests yielded essentially equal corrosion rates of 0.1 mils/year (mpy). Overall, no major difference in aqueous corrosion behavior was produced by the different heat treatments.

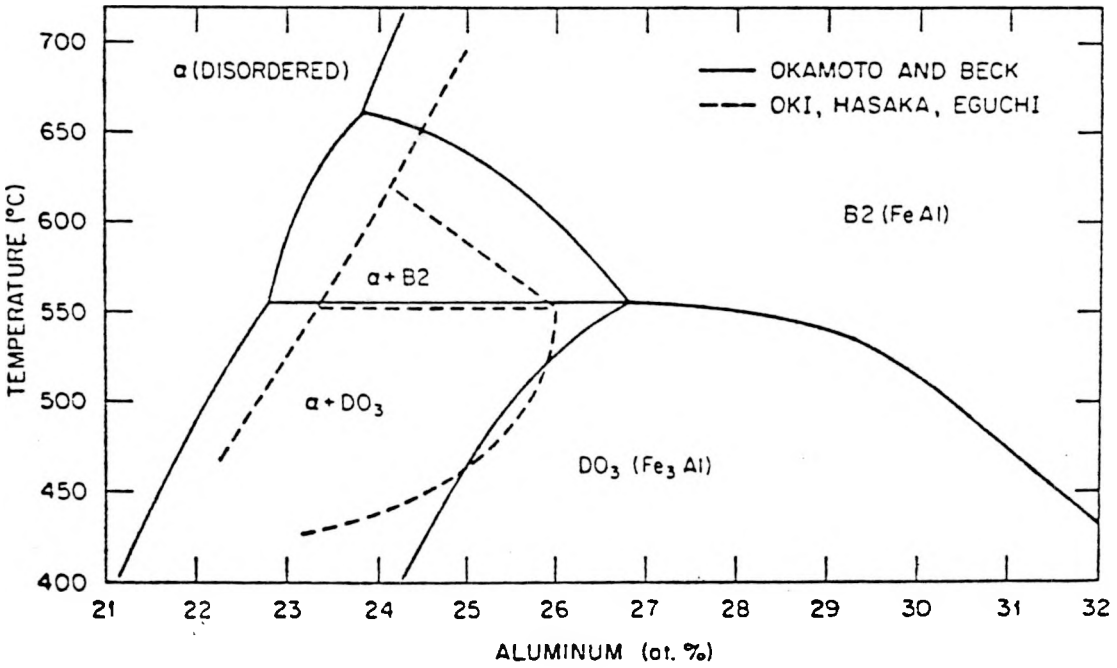

Fig. 8. Iron-Aluminum Phase Diagram[24]

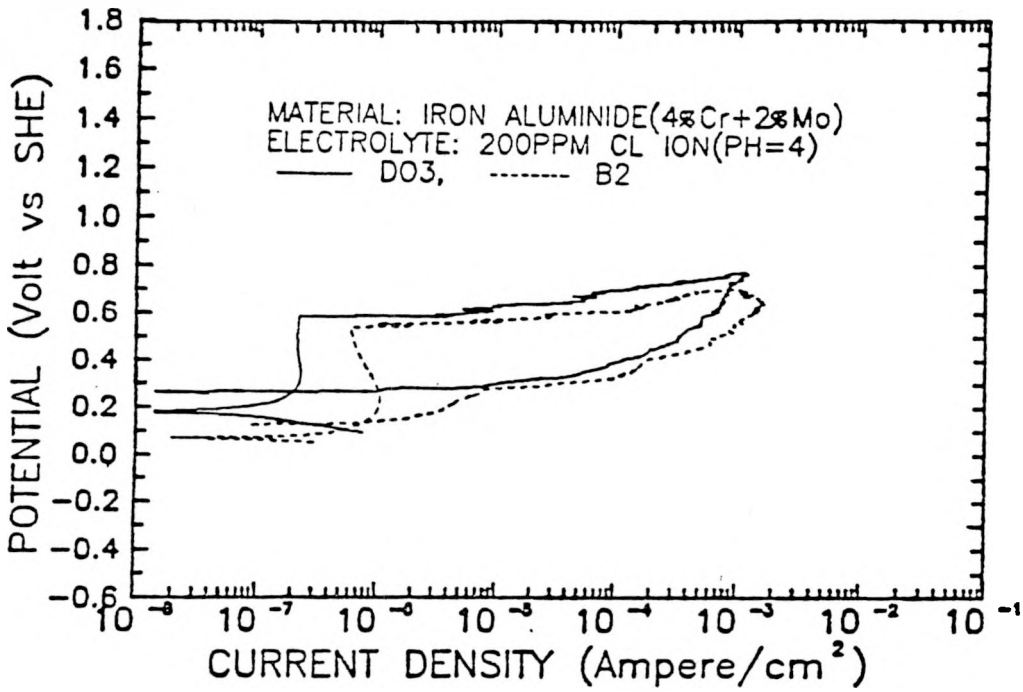

Fig. 9. Effects of Structure on Anodic Polarization Behavior

The next phase in the study involved evaluations of cyclic anodic polarization behavior and corrosion rates by the polarization-resistance method (600 mV/h scan rates) for certain iron aluminides in acid-chloride (200 ppm Cl^-, pH=4 (H_2SO_4)), thiosulfate (0.1M $Na_2S_2O_3$), and tetrathionate (0.1M $Na_2S_4O_6$) solutions. Selection of these electrolytes was based on the following rational. The acid-chloride solution was meant to reflect a somewhat aggressive acid-rain-type atmospheric-corrosion situation. The sulfur-compound solutions reflected the following situation. In the fossil energy-production area, the primary source of sulfur compounds is the fuel itself, and more directly, the fuel-combustion products. Any structural material exposed to the combustion products, as in flue-gas clean-up systems, may be susceptible to accelerated corrosion and stress-corrosion cracking (SCC) due to the sulfur compounds. Such structural components normally operating at elevated temperature may develop scales containing sulfides. During shutdown, e.g. for inspections, and upon exposure to the atmosphere, the sulfides can interact with moisture and oxygen to form aggressive sulfur-bearing acids. Of particular importance are the polythionic acids ($H_2S_xO_6$).[25-27] A number of investigators have indicated that the most aggressive polythionic-acid-component is tetrathionic acid ($H_2S_4O_6$).[28,29] This acid can be formed by adding $Na_2S_4O_6$ to water,

which undergoes hydrolysis to form the acid. An ion not formed in polythionic-acid solution, but closely related to the tetrathionate ion, is the thiosulfate ion ($S_2O_3^{2-}$).[30] It also has been linked to SCC problems in petroleum and electric-power industries.[29-32]

The iron aluminides evaluated, their compositions, and designations are given in Table 3. In all cases, the final heat treatment consisted of 1 hour at 750°C (air) followed by an oil quench. After creating the 0.1M solutions of $Na_2S_2O_3$ and $Na_2S_4O_6$, the pH values were measured to be 5 and 4, respectively. The polarization characteristics of the iron aluminides in the acid-chloride, thiosulfate, and tetrathionate solutions are shown in Figures 10,11 and 12, respectively. In the acid-chloride solution, passive behavior was observed for all materials until the localized-corrosion breakdown potential was exceeded. The breakdown potential was higher, and the passive-current-density lower, for the 5% Cr compositions (FA-129 and FA-133) than for the 2% Cr compositions (FA-136 and FA-84), indicating beneficial effects for the higher Cr level. The protection potentials were below the open-circuit corrosion potentials in all cases except for the FA-133 composition which contained, unlike the other compositions, 0.5% Mo. In this case, the two potentials were approximately the same, indicating improved resistance to initiation of localized corrosion. In the thiosulfate and tetrathionate solutions, Figures 11 and 12, only active corrosion behavior was observed, indicating no tendency to form protective passive films. Results of the polarization-resistance corrosion-rate measurements are given in Table 4. It is seen that all iron-aluminide compositions produced low corrosion rates in the acid-chloride solution (0.2-0.8 mpy) and high corrosion rates in both the thiosulfate and tetrathionate solutions (44-308 mpy).

Table 3. Compositions of Selected Iron Aluminides (at. %)

Materials	Fe	Al	Cr	C	Nb	B	Mo	Zr
FA129	65.8	28	5	0.2	1			
FA133	65.7	28	5	--	0.5	0.2	0.5	0.1
FA136	69.3	28	2	0.2	0.5			
FA84	69.95	28	2	--	--	0.05		

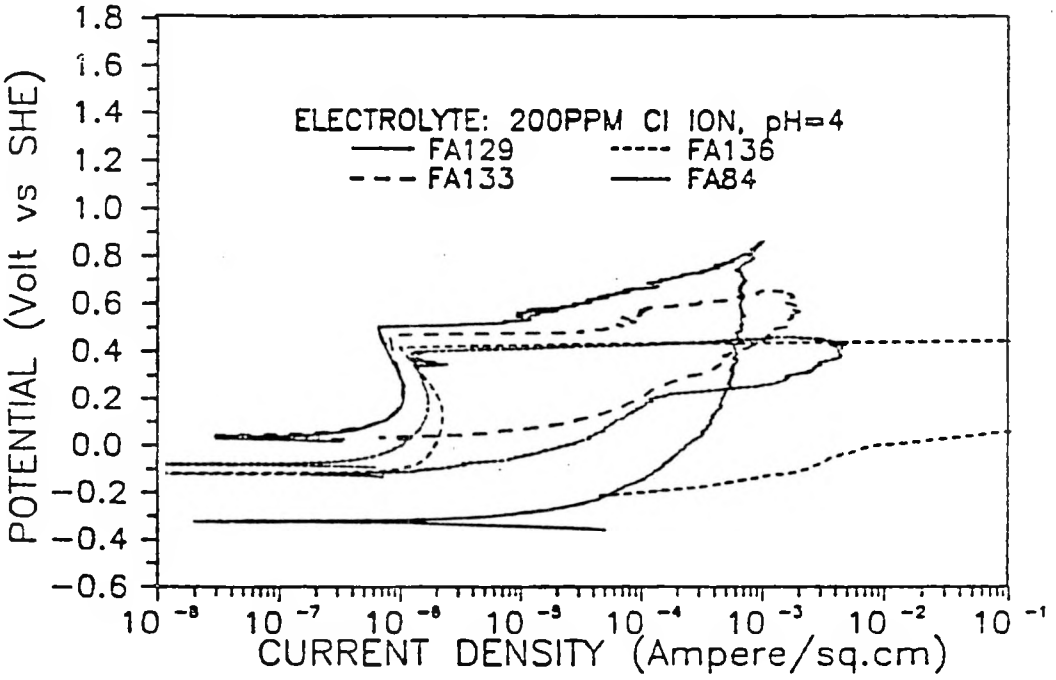

Fig. 10. Cyclic Anodic Polarization Behavior in Acid-Chloride Solution

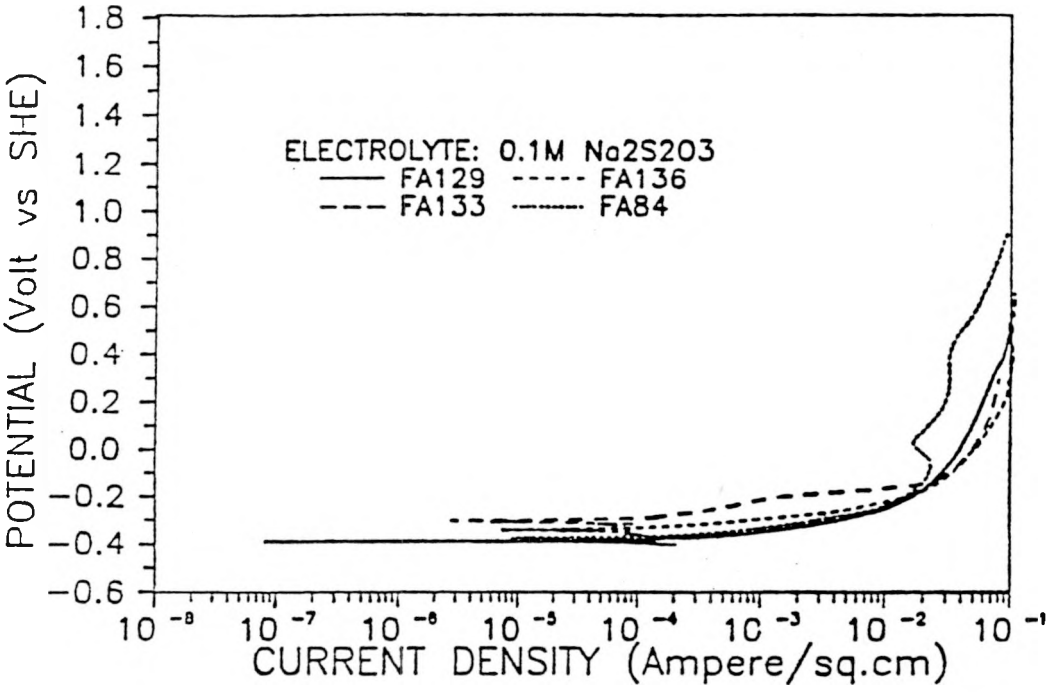

Fig. 11. Anodic Polarization Behavior in Thiosulfate Solution

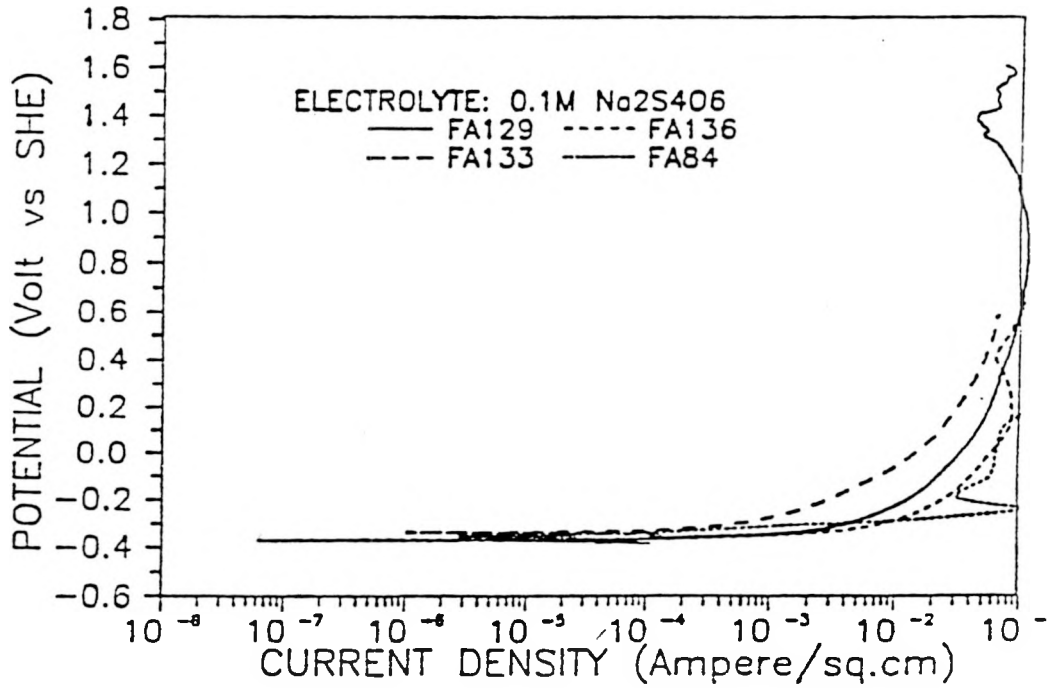

Fig. 12. Anodic Polarization Behavior in Tetrathionate Solution

Table 4. Corrosion Rates by the Polarization-Resistance Method

Solution	Corrosion Rate (mpy)			
	FA-129	FA-133	FA-136	FA-84
200 ppm Cl^-, pH = 4	0.2	0.2	0.8	0.4
0.1M $Na_2S_2O_3$	142	44	79	112
0.1M $Na_2S_4O_6$	94	91	96	308

Two additional iron-aluminide compositions were also evaluated in terms of polarization behavior in the acid-chloride solution. These compositions were patterned after FA-129 (Fe-28Al-5Cr-0.2C-1Nb), but one had a higher Nb concentration, 2 at.% vs. 1 at.%, the other a higher Cr concentration, 9 at.% vs. 5 at.%, with both adjustments being accomplished by reducing the Fe concentration. The resultant polarization curves are compared in Figure 13. Both the higher Cr and the higher Nb increased the breakdown potential; however, the protection potentials remained below the open-circuit corrosion potentials in both cases.

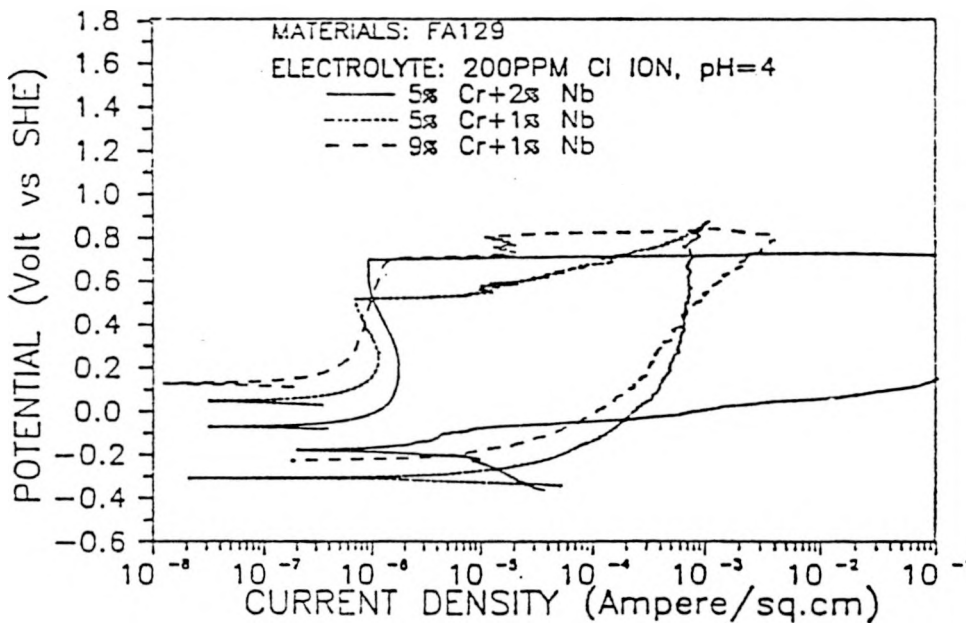

Fig. 13. Effects of Cr and Nb on Cyclic Anodic Polarization Behavior

At this stage in the project, two additional Mo-containing iron aluminides were produced at ORNL, FAL-1 w/o Mo and FAL-2 w/o Mo. The electrochemical corrosion characteristics of these iron-aluminide compositions, along with several other compositions as shown in Table 5, were evaluated in several different electrolytes. All received the 1 hour at 750 °C plus oil-quench (B2 stabilizing) heat treatment before evaluation.

Table 5. Chemical compositions of iron aluminides.

Material	Composition (atomic %)							
	Fe	Al	Cr	Mo	C	Nb	B	Zr
FA-84	70.0	28	2	-	-	-	0.005	-
FA-129	65.8	28	5	-	0.2	1	-	-
FA-140	60.0	28	4	2	-	-	-	-
FAL-1 w/o Mo	66.4	28	5	0.5	-	-	0.04	0.08
FAL -2 w/o Mo	65.9	28	5	1	-	-	0.04	0.08

In Figure 14, cyclic anodic polarization curves are presented for FA-129, FAL-1 w/o Mo, and FAL-2 w/o Mo in the aerated, pH = 4, 200 ppm Cl^- acid-chloride solution. The major effect was an increasing protection potential with increasing Mo concentration, indicating improved resistance to chloride-induced pitting corrosion.

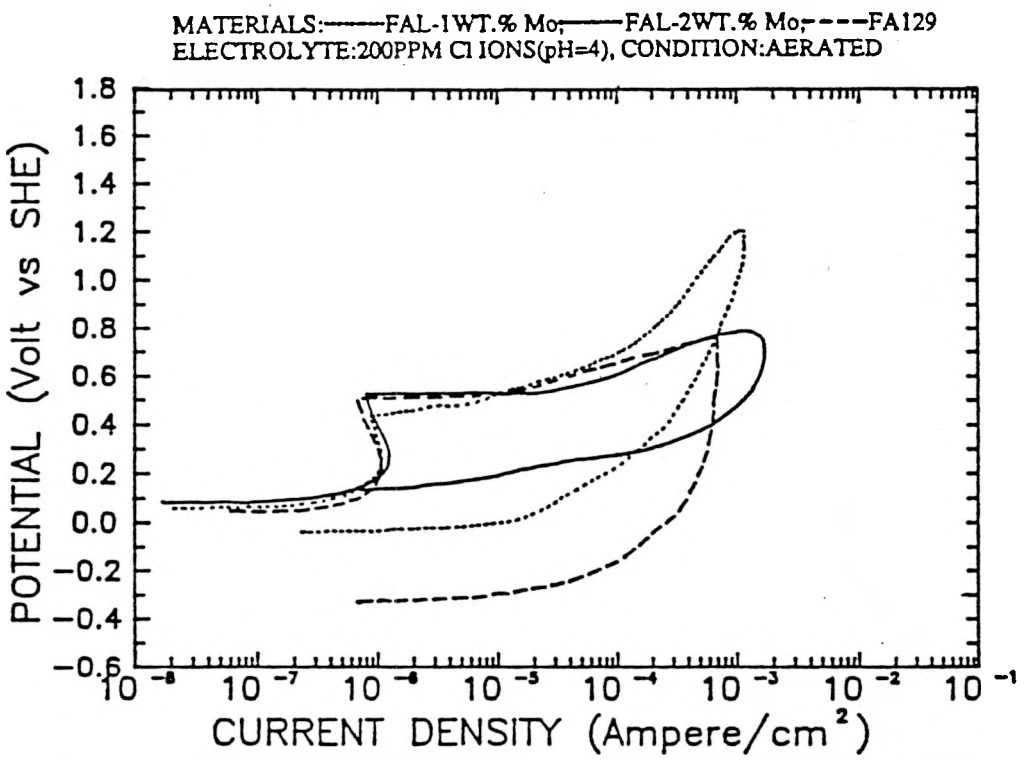

Fig. 14. Cyclic Anodic Polarization Behavior in Aerated, pH = 4, 200 ppm Cl^- Solution

In Figure 15, cyclic anodic polarization curves are given for FA-129, FA-140, and 304L and 316L stainless steel in aerated synthetic seawater ("Instant Ocean", Aquarium Systems, Mentor, Ohio). From these data, the corrosion potential (E_{corr}), pitting potential (E_{pit}), protection potential (E_{prot}), and the differences (E_{pit} - E_{corr}) and (E_{prot} - E_{corr}) are given in Table 6. The overall resistance to pitting corrosion increases as both (E_{pit} - E_{corr}) and (E_{prot} - E_{corr}) increase. The results in Table 6 indicate that FA-129 has the lowest resistance to pitting corrosion in synthetic seawater, that 316L has the highest resistance, and that FA-140 and 304L are generally comparable.

The cyclic anodic polarization results for FA-129, FA-140, and 304L stainless steel in aerated 1N sulfuric acid are given in Figure 16. Whereas the 304L passivated in this solution, both FA-129 and FA-140 exhibited active corrosion at high rates. The results of duplicate polarization-resistance measurements of the corrosion rates are given in Table 7.

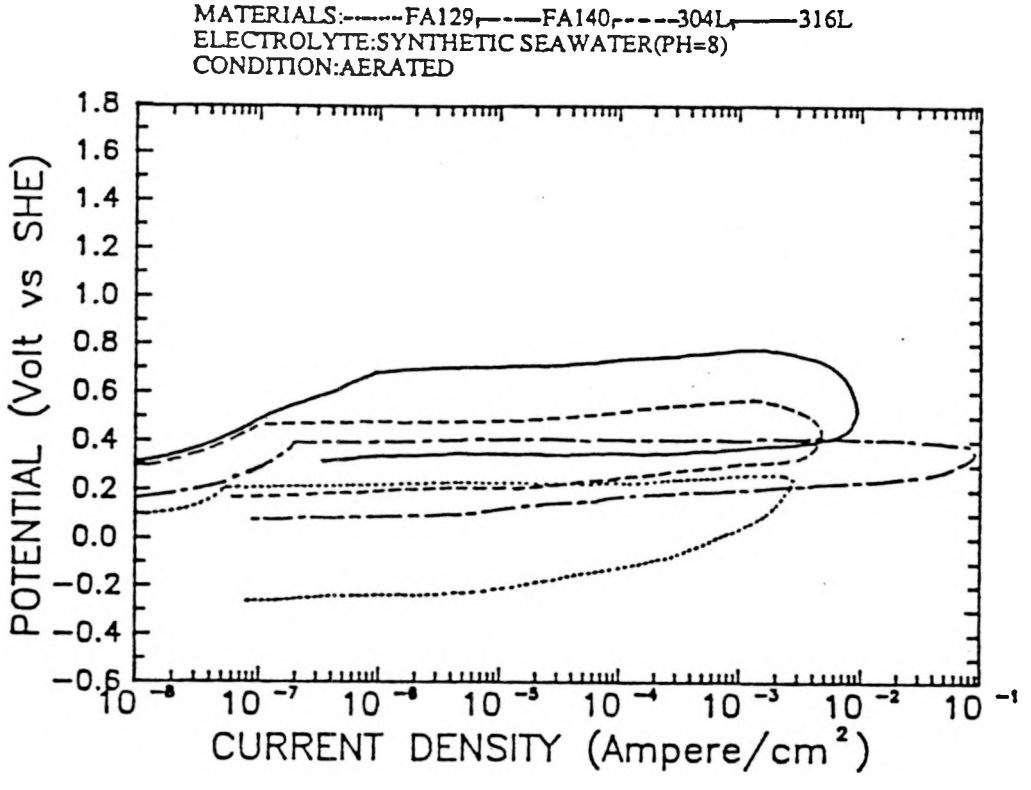

Fig. 15. Cyclic Anodic Polarization Behavior in Aerated Synthetic Seawater

Table 6. Electrochemical corrosion characteristics in aerated synthetic seawater.

Material	E_{pit} [mV (SHE)]	E_{prot} [mV (SHE)]	$(E_{pit}-E_{corr})$ [mV]	$(E_{prot}-E_{corr})$ [mV]
FA-129	90	200	-270	110	-360
FA-140	160	390	90	230	-70
304L	300	460	180	160	-120
316L	310	680	320	370	10

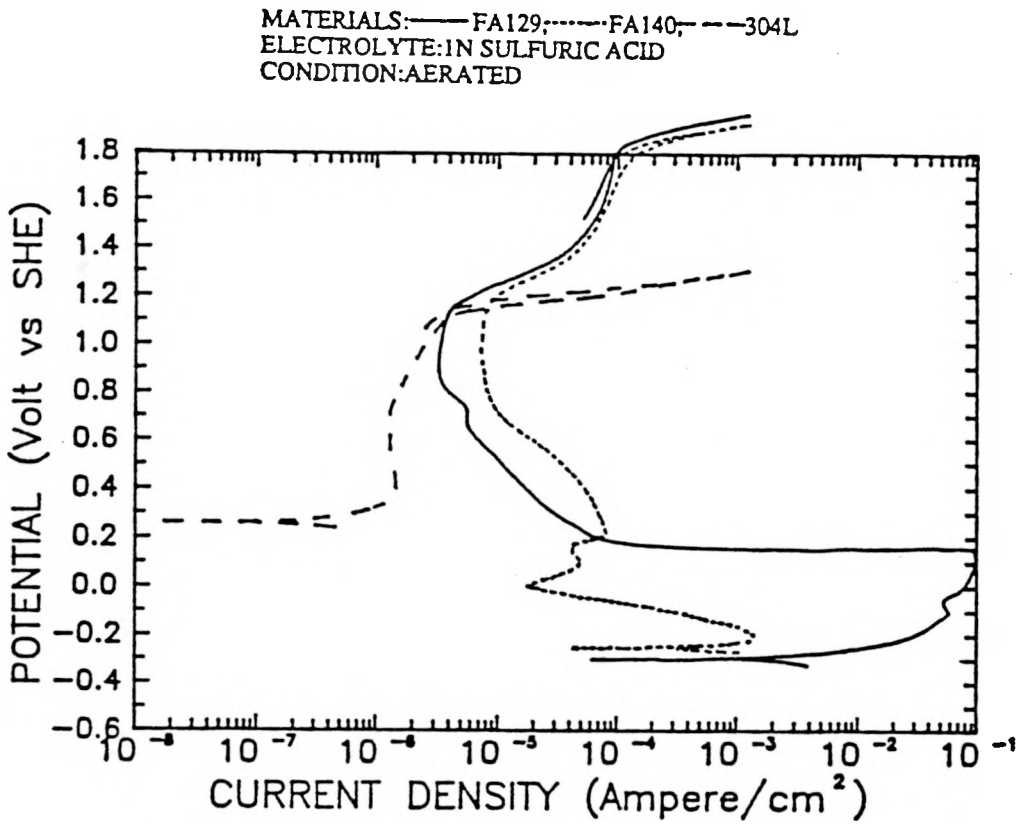

Fig. 16. Cyclic Anodic Polarization Behavior in Aerated 1N Sulfuric Acid

Table 7. Average Penetration Rates by Polarization-Resistance Measurements in Aerated 1N Sulfuric Acid.

Material	Average Penetration Rate (mpy) (Duplicate Measurements)
FA-129	613, 1460
FA-140	200, 511
304L	0.2, 0.2

Immersion Test Results

A number of the iron aluminides (Fe + 28 at. % Al) containing chromium and chromium-plus-molybdenum were studied by immersion methods in the acid-chloride solution (200 ppm Cl^-, pH=4 (H_2SO_4)). The surface preparation consisted of a final grinding step with 600 grit SiC paper, as was the case for all results presented in this report. Through cyclic anodic polarization testing, it had been observed that all of these materials passivated and produced low corrosion rates. It had also been observed, however, that the materials demonstrated varying degrees of susceptibility to localized corrosion. Since analysis of polarization behavior could not predict initiation times for localized corrosion, immersion tests were conducted whereby the initiation times were visually determined. The results are given in Table 8. Consistent with the polarization results, these immersion-test results further indicate the importance of both Cr and Mo in providing resistance to the initiation of localized corrosion.

Table 8. Immersion Test Results, Acid-Chloride Solution, Visual-Corrosion-Product Initiation Times

Material* (at. %)	Designation	Visual-Corrosion-Product (Localized) Initiation Times (days)
Fe-28 Al	FA-61	1
Fe-28 Al plus	-	-
2Cr	FA-77B	2
4Cr	FA-72C	27
6Cr	FA-78	27
2Cr - 1Mo	FA-86	2
2Cr - 2 Mo	FA-85	41
4 Cr-0.5 Mo	FA-138	2
4 Cr - 1 Mo	FA-139	>122**
4Cr - 2 Mo	FA140	>122**

*Air annealed: 1 hour at 850°C plus 2 days at 500°C, air-cooled

** Test stopped at 122 days

U-Bend Corrosion Cracking Tests

U-bend corrosion tests were performed on two iron-aluminide compositions, designated as FA-84 and FA-129, and containing 2 and 5 at.% Cr, respectively (see Table 5). In all cases, the final heat treatment consisted of 1 hour at 750°C (air) followed by an oil quench, which is believed to result in the B2 superlattice at room temperature. U-bend specimens were formed from strips measuring 119 x 10 x 0.76 mm. The specimens were first ground in the longitudinal direction through 600-grit SiC paper, and then deformed into the U shape with a fixture designed specifically for this purpose. The bend radius was 15.9 mm, resulting in a total strain of 0.024 (ASTM G 30), which exceeded the yield strengths of the iron aluminides. The legs of the U-bend specimens were secured with polyvinyl chloride bolts to avoid galvanic-corrosion effects.

The U-bend tests were conducted for a maximum time of 200 hours (when failure did not occur) in three electrolytes: acid-chloride (pH = 4 (H_2SO_4), 200 ppm Cl^- (NaCl)), 0.1M sodium thiosulfate ($Na_2S_2O_3$), and 0.1M sodium tetrathionate ($Na_2S_4O_6$). The pH values of the latter two solutions were measured to be 5 and 4, respectively. Justifications for selection of these electrolytes were presented in a previous section of this report.

Results of the first series of 200-hour U-bend corrosion tests are given in Table 9. In this series, the specimens were allowed to remain at their natural, freely-corroding, open-circuit corrosion potentials (E_{corr} values). It is seen that cracking did not occur in the acid-chloride solution within 200h for either the 2 or 5 % Cr iron alumindes. Furthermore, whereas localized corrosion was not evident for the 5 % Cr material (the entire surface remained bright and shiny), localized corrosion was readily apparent on the 2 % Cr material (although no cracks were initiated). The sulfur-compound solutions proved to be highly damaging to both iron-aluminide compositions, with severe corrosion and cracking failures occurring in both thiosulfate and tetrathionate solutions within 200 hours. Scanning-electron-microscopy analyses of the fracture surfaces indicated that the dominant cracking modes were transgranular for FA-84 (2 at. % Cr) and intergranular for FA-129 (5 at.% Cr).

Table 9. U-Bend Results at Open-Circuit Corrosion Potentials (E_{corr})

Material	Electrolyte	E_{corr}, Avg. (mV (SHE))	Results
FA-84 2 a/o Cr	Acid Chloride	(-200) → (-315)	No Cracking Localized Corrosion
	Thiosulfate	(-372) → (-315)	Cracking Failure, Transgranular
	Tetrathionate	(-410) → (-355)	Cracking Failure, Mode Unidentified Due to Severe Corrosion Products
FA-129 5 a/o Cr	Acid Chloride	(-40) → (+ 290)	No Cracking No Localized Corrosion
	Thiosulfate	(-390) → (-300)	Cracking Failure, Intergranular
	Tetrathionate	(-415) → (-395)	Cracking Failure, Intergranular

A second series of U-bend corrosion tests were performed under identical experimental conditions, except that the specimen potentials (E) were potentiostatically controlled. In terms of background information, it is helpful to describe the conditions that exist as a function of electrochemical potential. Under freely-corroding conditions (E = E_{corr}), the corrosion rate (or metal-oxidation rate) is equal to the cathodic-reactant

reduction rate. At anodic potentials ($E>E_{corr}$), the corrosion rate is higher than the reduction rate; and at cathodic potentials ($E<E_{corr}$), the reduction rate is higher than the corrosion rate. Furthermore, the degree of imbalance increases as E is forced further away from E_{corr}. Thus, higher anodic potentials progressively accelerate the corrosion reaction, and lower (more-negative) cathodic potentials progressively accelerate the reduction reaction(s). In addition to the E_{corr} values, the following applied potentials were investigated: (a) anodic, +300 mV (SHE); and (b) cathodic, -900, -1000, and -1500 mV (SHE). The locations of these potentials are illustrated in Figure 17 with reference to the anodic and cathodic polarization curves of FA-129 in the acid-chloride solution. At the cathodic potentials, it must be recognized that different reduction reactions occur over different potential ranges. The possible reduction reactions are identified as: (A) $O_2 + 4H^+ + 4e \rightarrow 2H_2O$, (B) $2H^+ + 2e \rightarrow 2H$, and (C) $2H_2O + 2e \rightarrow 2H + 2(OH)^-$. Only reaction A will occur at potentials greater than -236 mV(SHE); whereas below this value, all three reactions will occur. Thus, atomic hydrogen is generated at the specimen surfaces only at potentials less than -236 mV (SHE). (A corollary to this statement is that if E_{corr}, the freely-corroding potential, is greater than -236 mV(SHE), which it has been for all iron aluminides tested without stress application in the acid-chloride solution, no hydrogen is generated at the surface.). Kinetically, based on the shape of the typical cathodic polarization curve in Figure 17 for the acid-chloride solution (pH = 4), it was observed that reaction A dominated the cathodic reactions down to a potential of approximately -550 mV(SHE), with the oxygen diffusion limit occurring at approximately 30 $\mu A/cm^2$. Within this range, reactions B and C occurred below -236 mV(SHE), but at slower rates than reaction A. Below -550 mV(SHE), reaction C dominated the cathodic reactions. At the applied cathodic potentials of -900,-1000, and -1500 mV(SHE), hydrogen gas-bubble generation at the specimen surfaces was observed to occur at progressively higher rates.

Results of the series of U-bend corrosion tests with potentiostatically-controlled potentials are presented in Table 10. At the anodic potential of +300 mV(SHE), localized corrosion initiated on both the 2 and 5 at.% Cr iron aluminides. However, cracking failures did not occur for either material. Indeed, localized corrosion was so severe for the 2 % Cr material that through-thickness penetrations were evident at several sites; yet the U-bend specimens did not crack and mechanically fail. At the applied cathodic potentials, for the 2 % Cr iron aluminide, cracking did not occur within 200h at -900 mV(SHE), but did occur in 45h (average) at -1000 mV(SHE), and 17h (average) at -1500 mV(SHE).

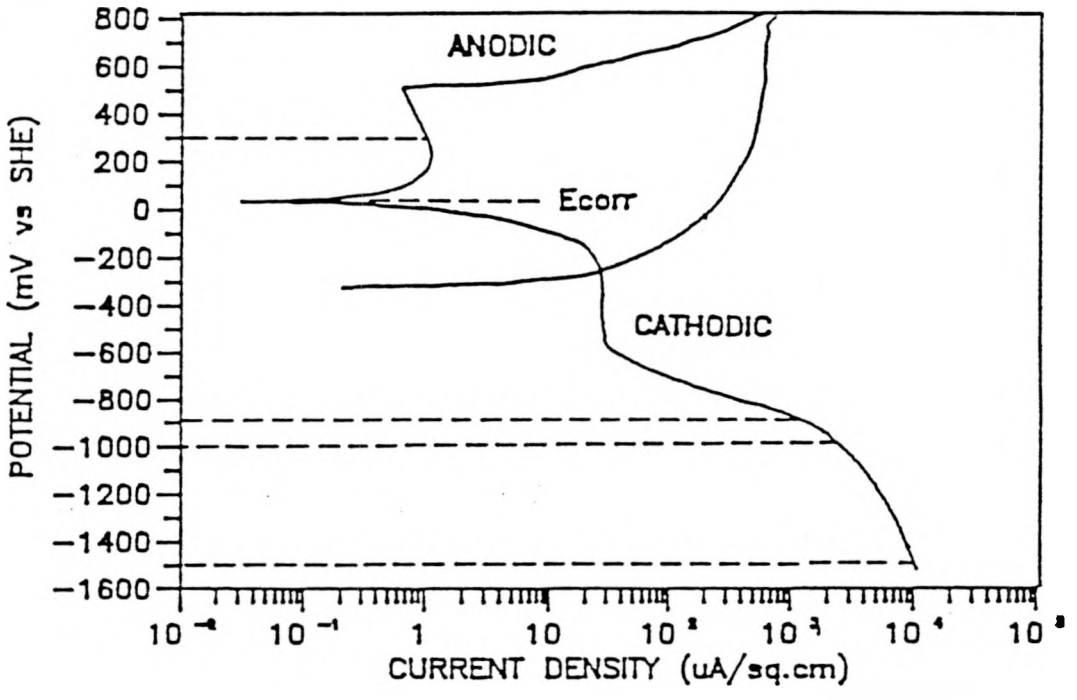

Fig. 17. Anodic and Cathodic Polarization Curves for FA-129 Iron Aluminide in Acid-Chloride Solution. Applied Anodic and Cathodic Potentials are Identified by Dashed Lines.

For the 5 % Cr iron aluminide, cracking did not occur within 200h at any of the applied cathodic potentials.

In summary, the 200h U-bend corrosion tests of the two iron-aluminide compositions (2 and 5 at.% Cr), under freely-corroding conditions, produced cracking failures in thiosulfate and tetrathionate solutions, but not in the acid-chloride solution. Additional tests in the acid-chloride solution at an applied anodic potential (corrosion acceleration) did not produce cracking failures for either the 2 or 5 % Cr iron aluminides. Further testing at applied cathodic potentials sufficiently active to generate hydrogen at the

Table 10. U-bend Test Results in Acid-Chloride Solution Over a Range of Applied Potentials

Material	E(Applied) (mV (SHE))	Results	No. of Tests
FA-84 2 a/o Cr	+ 300	No Cracking Localized Corrosion	3
	(-200) → (-315) E_{corr}	No Cracking Localized Corrosion	2
	-900	No Cracking	2
	-1000	Cracking Failure, Transgranular (45 h, avg.)	2
	-1500	Cracking Failure (17 h, avg.)	2
FA-129 5 a/o Cr	+ 300	No Cracking Localized Corrosion	2
	(-40) → (+ 290) E_{corr}	No Cracking No Localized Corrosion	2
	-900	No Cracking	2
	-1000	No Cracking	2
	-1500	No Cracking	1

specimen surfaces (while simultaneously decreasing the corrosion rate) produced cracking failures in the 2 % Cr iron aluminide at the more severe cathodic potentials, but did not produce cracking failures in the 5 % Cr iron aluminide.

The results indicated that the iron aluminides evaluated in this part of the study are highly susceptible to environmentally-assisted cracking in thiosulfate and tetrathionate solutions under freely-corroding conditions.

The results also indicated that the iron aluminides are susceptible to environmentally-assisted cracking in the acid-chloride solution, that the mechanism is related to hydrogen-embrittlement effects rather than anodic-dissolution effects (i.e. stress corrosion per se), and that higher Cr levels are beneficial in minimizing this form of environmental cracking.

A critical question at this point is whether the iron aluminides would ever undergo environmental cracking under the freely-corroding condition (E_{corr}) during U-bend-type testing (constant strain, approximately constant stress) in the acid-chloride solution. Recall that the time duration in the present study was 200h. Also recall from previous discussion that E_{corr} must be less than -236 mV(SHE) at pH = 4 in order for the cathodic reaction to produce hydrogen during the corrosion process. Based on the E_{corr} values in Table 10 and the nature of the cracking mechanism revealed in this study, one must reasonably conclude that cracking could occur under freely-corroding conditions during a U-bend-type test (and by implication, during a constant-stress-type situation) for the 2 % Cr iron aluminide at a time period greater than 200h, but would not occur for the 5 % Cr iron aluminide as long as E_{corr} remained as high as shown in Table 10. However, the 5 % Cr iron aluminide is susceptible to localized corrosion, and based on the results of Table 8, localized corrosion could initiate in approximately 27 days (648h). When localized corrosion initiates, E_{corr} normally decreases, and in the present case, it could decrease sufficiently to result in hydrogen generation, which subsequently could result in cracking. It is noted in Table 8 that Mo additions decrease the susceptibility to localized corrosion, and by inference, could decrease the susceptibility to environmental cracking.

Consistent with the above arguments, it is noted in Table 9 that the E_{corr} values during U-bend testing in thiosulfate and tetrathionate solutions were always less than -236 mV(SHE), meaning that hydrogen was being generated at the surfaces during the corrosion process. Also, as previously described, cracking failures occurred within 200h in all cases. Previous work showed that the iron aluminides do not passivate in these solutions (Figures 11 and 12), an effect which not only leads to high corrosion rates, but also causes a low E_{corr}, hydrogen generation, and cracking.

With regard to the promising responses of the iron aluminides, especially the 5 % Cr material, in the acid-chloride solution under U-bend-test conditions, a note of caution must be expressed. A different situation could exist during a slow-strain-rate corrosion (SSRC) test. Under these conditions, fresh, nonpassivated (nonprotected) surfaces are continuously being exposed to the electrolyte as a consequence of dislocation movement to the surface during plastic deformation. For short periods of time, until the fresh surfaces self-passivate, E_{corr} could be quite active -- sufficiently active to produce hydrogen locally, which in turn could lead to hydrogen-embrittlement cracking and loss of ductility. Because of these possibilities and concerns, SSRC tests were initiated as part of this overall program.

Slow-Strain-Rate Corrosion (SSRC) Tests

The SSRC tests were conducted at freely-corroding open-circuit potentials and at a potentiostatically-controlled cathodic potential of -1500 mV(SHE). The latter potential was sufficiently negative to generate significant amounts of hydrogen at the specimen surfaces. The test cell consisted of a glass vessel with polyvinyl chloride top and bottom sections containing access ports with compression fittings. Two platinum counter electrodes, one on either side of the specimen, and a Luggin probe were introduced into the cell through the compression fittings. A saturated Ag/AgCl reference electrode was employed in monitoring the electrochemical potential of the sample. The tensile force applied to the sample was monitored through measurement of a load-cell output, and the cross-head displacement was monitored through measurement on a multiple-turn variable resistor placed within the cross-head drive system. During a given test procedure, the applied force, crosshead displacement, and either the specimen corrosion potential (freely-corroding condition) or the reduction current density (constant cathodic potential, -1500 mV(SHE)) were continuously recorded with a computer system.

The initial SSRC evaluations were performed with a test-specimen geometry as supplied by Oak Ridge National Laboratory (ORNL). The specimen geometry was exactly the same as used at ORNL in their tensile-testing program (Figure 18). The specimens were annealed for 1 hour at 750°C (air) and oil quenched. The surfaces and edges were ground to a 600-grit SiC finish immediately prior to testing. The SSRC tests were conducted in pH = 4, 200 ppm Cl^- solution at a strain rate of 1.2×10^{-6}/s. For comparison, the tensile-testing strain rate at ORNL was 3.3×10^{-3}/s, approximately 2700 times faster.

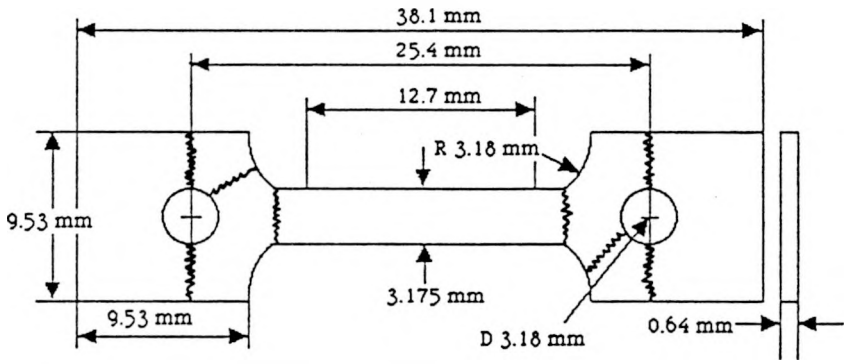

Fig. 18. Tensile Specimen Geometry Employed at ORNL, with Slow-Strain-Rate-Corrosion Fracture Locations Identified

The SSRC testing program has been plagued with difficulties, which still may not be totally resolved. With the ORNL tensile-specimen geometry, the SSRC testing procedure produced fractures outside of the gage-section area. As indicated in Figure 18, the fractures occurred either at the pin-hole locations or where the gripping-section filet merged with the gage section. Although this mode of failure occasionally occurred during tensile testing at ORNL (strain rate = 3.3×10^{-3}/s), it occurred 15 times in 16 tests during SSRC testing (strain rate = 1.2×10^{-6}/s). The basic problem was that with this mode of failure, valid % elongation values could not be obtained under the SSRC testing procedures. Much effort and time were spent in trying to solve this testing problem (each SSRC test required 20-60 hours). Specific actions were as follows, in chronological order: the testing machine was even-more carefully aligned, the specimen edges and pin-hole edges were polished to minimize stress-concentration effects, and finally, reinforcement sections were spot welded to the gripping sections to reduce the stress levels at these locations. None of these actions, involving 16 different tests, produced the desired gage-section fractures in a reproducible manner. A tentative conclusion based on these experiences is that the iron aluminides under evaluation (FA-84 and FA-129) are much more sensitive to stress-concentration effects (notch effects) at slow strain rates in a corrosive medium than at the higher strain rate previously employed at ORNL for tensile testing in air.

As an additional action to solve the SSRC testing problem, the as-supplied ORNL tensile specimens were ground to a series of different geometries, with the primary goal being to reduce the width of the gage section and thereby reduce the level of stress in the gripping sections. The SSRC test-specimen geometry being employed at the present time is shown in Figure 19. Its nominal gage-section width is 1.78 mm as compared to the original width of 3.18 mm. Furthermore, the width of the center portion of the present SSRC test-specimen gage section was reduced by an additional 0.076 mm. The SSRC test results with this specimen geometry, at the freely-corroding potential (E_{corr}) and at the cathodic hydrogen-production potential of -1500 mV(SHE), are given in Table 11. The tests on FA-84 (2 a/o Cr) at E_{corr} are considered valid tests since the fractures occurred near the centers of the gage sections. Note that the % elongation values are reasonably high (~13 %). The other test results in Table 11 are still somewhat questionable. Although the fractures occurred within the 0.5-inch gage sections, the fracture sites were close to one of the ink-line gage marks, which could have resulted in

somewhat lower measured % elongation values. Given this note of caution, the results in Table 11 at E_{corr} appear to indicate a more severe environmental embrittlement effect for

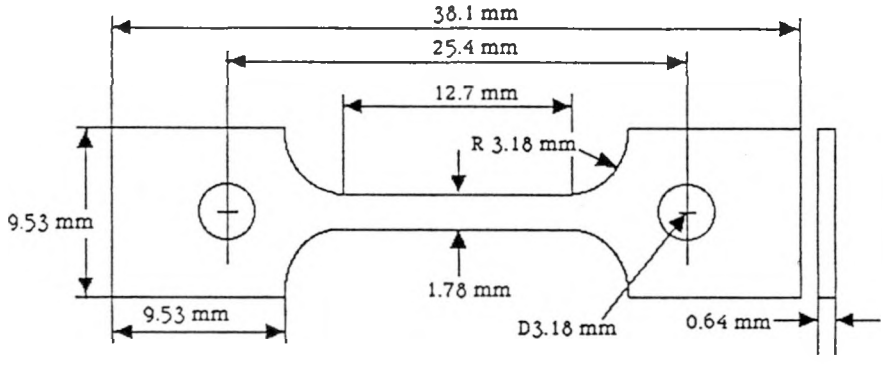

Fig. 19. Current Slow-Strain-Rate Corrosion Test-Specimen Geometry

Table 11. Slow-Strain-Rate Corrosion Test Results

Material	Potential	Time To Fracture (hours)	Fracture Stress (MPa)	% Elongation
FA-84	E_{corr}	59	724	12.8
		-	-	12.5
		71	758	13.7
FA-129	E_{corr}	16	655	3.4
		22	552	4.2
		31	552	5.7
FA-84	-1500 mV (SHE)	11	414	1.6
		10	386	2.5
FA-129	-1500 mV (SHE)	9	379	0.8
		9	414	2.5

FA-129 (5 at.% Cr) than for FA-84 (2 at.% Cr). More data must be collected before a definite conclusion is drawn. At the applied hydrogen-producing cathodic potential (-1500 mV (SHE)), the % elongation values for both materials decreased -- a result consistent with the hydrogen-embrittlement mechanism.

SUMMARY AND CONCLUSIONS

1. Initial experiments in 1H NCl and 1N H_2SO_4 acids, 3.5 wt.% NaCl, and 1N NaOH for compositions (at. %) of Fe-28Al (FA-61), FA-28Al-2Cr (FA-77B), FA-28Al-4Cr (FA-72C) and FA-28Al-6Cr (FA-78) generally indicated active corrosion at high rates in the strong acids, passivation with a tendency for localized corrosion in the NaCl solution, and passivation with no localized-corrosion susceptibility in the strongly-basic NaOH solution.

2. An intermediately-aggressive acid-chloride solution (pH = 4, 200 ppm Cl^-) was employed for better differentiation of the Cr effect in the above alloys. Increasing Cr levels were found to increase the localized-corrosion breakdown potential (electrochemical tests) and therefore provide increasing resistance to initiation of localized corrosion. However, protection potentials were found to be, in all cases, lower than the corrosion potentials, indicating that localized corrosion could still initiate after incubation periods of time. Immersion tests confirmed these electrochemical-based predictions.

3. It was recommended that Mo additions be made to the Fe-28Al-Cr compositions for possible improvements in localized-corrosion (pitting/crevice corrosion) resistance. Mo additions were found to increase the protection potential, thereby indicating significant improvements. Immersion tests confirmed these results. The most resistant composition (at. %) was Fe-28Al-4Cr-2Mo (FA-140).

4. Prior corrosion experiments had been conducted on iron aluminides that had received a heat treatment to produce the DO_3 superlattice (1h at 850°C plus 2d at 500°C). ORNL investigators determined that a different heat treatment (1h 750°C, oil-quench) produced higher room-temperature ductilities. The new heat treatment produced the B2 superlattice structure. A brief electrochemical polarization study

indicated only minor differences in corrosion response due to the two different heat treatments.

5. The electrochemical corrosion properties of a series of iron aluminides (FA-84, FA-129, FA-133, FA-136) were evaluated and compared in the acid-chloride solution (pH = 4, 200 ppm Cl^-) and in two sulfur-compound solutions (0.1 M $Na_2S_2O_3$ and 0.1M $Na_2S_4O_6$). Passivation developed for all compositions in the acid-chloride solution, with indicated susceptibilities for localized corrosion. The composition indicated to have the greatest resistance to localized corrosion (of the four evaluated in this part of the study) was FA-133, the only one containing Mo (0.5 at.%). All four compositions underwent active corrosion at high rates in both sulfur-compound solutions.

6. Two additional Mo-containing iron aluminides were developed at ORNL, FAL-1 w/o Mo (0.5 at.% Mo) and FAL-2 w/o Mo (1 at.% Mo). The electrochemical corrosion characteristics of these compositions were evaluated in the acid-chloride solution. Again, the Mo additions were found to be effective in significantly improving the resistance to localized corrosion, with the higher Mo concentration being more effective.

7. Selected iron aluminides were electrochemically evaluated in synthetic seawater and 1N H_2SO_4, and compared to stainless steels. In synthetic seawater, FA-129 (Fe-28Al-5Cr-0.2C-1Nb), FA-140 (Fe-28Al-4Cr-2Mo), AISI Type 304L, and AISI 316L were evaluated. In terms of localized corrosion susceptibility, the most susceptible material was FA-129, FA-140 and 304L were comparable, and 316L the was least susceptible. In 1N sulfuric acid, the materials evaluated were FA-129, FA-140 and 304L. Both iron aluminides underwent active corrosion at high rates, whereas the 304L passivated with a very low corrosion rate.

8. U-bend corrosion tests were conducted on two iron aluminides (at. %), FA-84 (Fe-28Al-2Cr-0.05B) and FA-129 (Fe-28Al-5Cr-0.2C-1Nb), in the acid-chloride solution and in the two sulfur-compound solutions, first at the respective open-circuit potentials. In the 200h tests, cracking occurred for both aluminides in both sulfur-compound solutions. For these combinations, the corrosion potentials

were sufficiently active to produce hydrogen at the specimen surfaces. In the acid-chloride solution, cracking did not occur for either iron aluminide; however, for FA-84 (2% Cr), the corrosion potential, although not as active as in the sulfur-compound solutions, was sufficiently active to produce hydrogen. U-bend corrosion tests were also conducted in the acid-chloride solution at a potentiostatically-controlled anodic potential and at three potentiostatically-controlled cathodic potentials selected to produce increasing amounts of hydrogen at the specimen surfaces. Cracking only occurred within the 200h testing period for the lower-Cr material (FA-84) and only at the two more severe cathodic potentials. These results indicated that the cracking was due to hydrogen embrittlement (not stress corrosion per se) and that increasing Cr concentration would minimize this cracking phenomenon. Although not evaluated, it was argued that Mo additions would further minimize the cracking phenomenon by increasing the passive-film stability.

9. Slow-strain-rate corrosion (SSRC) tests were conducted to further investigate the cracking phenomenon under aqueous-corrosion conditions; specifically, the ductility under these conditions was used as an indicator of cracking susceptibility. Whereas under U-bend conditions the passive film remains undisturbed by mechanical effects, under SSRC tests the passive film is continuously disrupted during the plastic-strain process (dislocation movement to the surface). Two iron aluminides were evaluated, FA-84 (Fe-28Al-2Cr-0.05B) and FA-129 (Fe-28Al-5Cr-0.2C-1Nb), in the acid-chloride solution at the open-circuit corrosion potentials and at the most severe potentiostatically-controlled hydrogen-producing cathodic potential employed in the prior U-bend tests. The ORNL tensile-specimen geometry was initially employed for SSRC testing. However, fractures occurred outside the gage section, and therefore invalidated the SSRC tests. These results indicated an enhanced notch effect under SSRC testing conditions which was not observed at ORNL during higher-strain-rate tensile testing in air. A series of different specimen geometries were evaluated to obtain valid SSRC test results. With apparently valid results (although not totally satisfactory), at the open-circuit corrosion potentials, the lower-Cr material (FA-84) produced higher ductilities, ~13% elongation, than the higher-Cr material (FA-129), ~4.5 % elongation. Under the hydrogen-charging cathodic potential, the ductilities of both

materials decreased to ~2% -- a result consistent with the hydrogen embrittlement mechanism. More work should be devoted to the SSRC testing program to develop a better understanding of these overall results.

REFERENCES

1. J. H. DeVan, pp. 107-15 in Oxidation of High-Temperature Intermetallics, ed. T. Grobstein and J. Doychak, The Minerals, Metals and Materials Society, 1989.
2. J. L. Smialek, J. Doychak, and D. J. Gaydosh, pp. 83-95 in Oxidation of High-Temperature Intermetallics, ed. T. Grobstein and J. Doychak, The Minerals, Metals and Materials Society, 1989.
3. J. F. Nachman and W. J. Buehler, Naval Ordnance Laboratory NAVORD Report 4130 (December 5, 1955).
4. F. X. Kayser, Ford Motor Company, WADC-TR-57-298, 1957.
5. E. R. Duffy and J. F. Nachman, Bureau of Mines Open File Report 112-76 (U.S. Dept. of Commerce, National Technical Information Service PB-259-253) June 1976.
6. R. G. Bordeau, AFWAL-TR-87-4009, Air Force Weight Aeronautical Laboratories, Wright-Patterson Air Force Base, Ohio, May 1987.
7. W. R. Kerr, Metall. Trans. 17A, 2298 (1986).
8. C. G. McKamey, J. A. Horton, and C. T. Liu, pp. 321-27 in MRS Symp. Proc., Vol. 81, High Temperature Ordered Intermetallic Alloys, ed. N. S. Stoloff, C. C. Koch, C. T. Liu, and O. Izumi, 1987.
9. G. Culbertson and C. S. Kortovich, AFWAL-TR-4155, Air Force Wright Aeronautical Laboratories, Wright-Patterson Air Force Base, Ohio, March 1986.
10. M. G. Mendiratta, S. K. Ehlers, D. K. Chatterjee, and H. A. Lipsitt, Metall. Trans. 18A, 283 (1987).
11. J. A. Horton, C. T. Liu, and C. C. Koch, pp. 309-21 in High Temperature Alloys: Theory and Design, ed. J. O. Stiegler, AIME , 1984.
12. R. G. Bordeau, AFWL-TR-87-4009, Development of Iron Aluminides, Air Force Wright Aeronautical Laboratories, Wright-Patterson Air Force Base, Ohio, May 1987.
13. M. G. Mendiratta, S. K. Ehlers, D. M. Dimiduk, W. R. Kerr, S. Mazdiyasni, and H. A. Lipsitt, pp. 393-404 in MRS Symp. Proc. Vol. 81, High Temperature Ordered Intermetallic Alloys, ed. N. S. Stoloff, C. C. Koch, C. T. Liu, and O. Izumi, 1987.

14. M. G. Mendiratta and H. A. Lipsitt, pp. 155-62 in MRS Symp. Proc. Vol. 39, High Temperature Ordered Intermetallic Alloys, ed. C. C. Koch, C. T. Liu, and N. S. Stoloff, 1985.
15. R. S. Diehm. M. P. Kemppainen, and D. E. Mikkola, Mater. Man. Proc. 4(1), 61 (1989).
16. V. K. Sikka, C. G. McKamey, C. R. Howell, and R. H. Baldwin, ORNL/TM-11465 (March 1990).
17. C. G. McKamey, C. T. Liu, J. A. Horton, and S. A. David, "Development of Iron Aluminides," pp. 275-284 in Fossil Energy AR&TD Materials Program Semiannual Progress Report for the Period Ending March 21, 1988, ORNL.FMP-88/1 (July 1988).
18. C. G. McKamey, J. A. Horton, and C. T. Liu, Scripta Metall. 22 (1988) 1679.
19. C. G. McKamey, J. A. Horton, and C. T. Liu, J. Mater. Res. 4(5) (1989) 1156.
20. C. T. Liu, E. H. Lee, and C. G. McKamey, Scripta Metall. 23 (1989) 875.
21. C. T. Liu, C. G. McKamey, and E. H. Lee, Scripta Metall. 24 (1990) 385.
22. C. T. Liu and C. G. McKamey, pp. 133-151 in High Temperature Aluminides and Intermetallics, ed. S. H. Whang, C. T. Liu, D. P. Pope. and J. O. Stiegler, The Minerals, Metals and Materials Society, 1990.
23. C. G. McKamey and C. T. Liu, "Chromium Addition and Environmental Embrittlement in Fe_3Al," submitted to Scripta Metall., August 20, 1990.
24. P. R. Swann, W. R. Duff, "The Diagram of State for Iron-Aluminum Solid Solutions," Transactions TMS-AIME, vol. 245, pp. 851-853 (1969).
25. S. Ahmad, M. L. Mehta, S. K. Saraf, and I. P. Saraswat, ":Effect of Polythionic Acid Concentration on Stress Corrosion Cracking of Sensitized 304 Austenitic Stainless Steel," Corrosion, Vol. 39, No. 8, 333 (1983).
26. S. Ahmad, M. L. Mehta, S. K. Saraf, and I. P. Saraswat, "Anodic Polarization Characteristics of Sensitized 304 Austenitic Stainless Steel in Polythionic Acid Environment," Corrosion, Vol. 39, No. 8, 330 (1983).
27. R. C. Scarberry, S. C. Pearman, and J. R. Crum, Corrosion, Vol. 32, p. 401 (1976).
28. P. H. Berge and J. L. Donati, Nuclear Technology, Vol. 55, p. 88 (1981).
29. R. C. Newman and K. Sieradzki, "Electrochemical Aspects of Stress-Corrosion Cracking of Sensitized Stainless Steels," Corrosion Science, Vol. 23, pp. 363-378 (1983).

30. H. H. Horowitz, "Chemical Studies of Polythionic Acid Stress Corrosion Cracking," Corrosion Science, Vol. 23, pp. 353-362 (1983).

31. R. C. Newman, R. Roberge, and R. Bandy, "Environmental Variables in the Low Temperature Stress Corrosion Cracking of Inconel 600," Corrosion, Vol. 39, No. 10, 386 (1983).

32. R. Bandy, R. Roberge, and R. C. Newman, "Low Temperature Stress Corrosion Cracking of Sensitized Inconel 600 in Tetrathionate and Thiosulfate Solutions," Corrosion, Vol. 39, No. 10, 391 (1983).

APPENDIX: DISTRIBUTION LIST

DISTRIBUTION

AIR PRODUCTS AND CHEMICALS
P.O. Box 538
Allentown, PA 18105
S. W. Dean
S. C. Weiner

ALBERTA RESEARCH COUNCIL
Oil Sands Research Department
P.O. Box 8330
Postal Station F
Edmonton, Alberta
Canada T6H5X2
L. G. S. Gray

ALLISON GAS TURBINE DIVISION
P.O. Box 420
Indianapolis, IN 46206-0420
P. Khandelwal (Speed Code W-5)
R. A. Wenglarz (Speed Code W-16)

ARGONNE NATIONAL LABORATORY
9700 S. Cass Avenue
Argonne, IL 60439
K. Natesan

ARGONNE NATIONAL LABORATORY-WEST
P.O. Box 2528
Idaho Falls, ID 83403-2528
S. P. Henslee

AVCO RESEARCH LABORATORY
2385 Revere Beach Parkway
Everett, MA 02149
R. J. Pollina

BABCOCK & WILCOX
1562 Beeson St.
Alliance, OH 44601
T. I. Johnson
T. Modrak

BABCOCK & WILCOX
Domestic Fossil Operations
20 South Van Buren Avenue
Barberton, OH 44023
M. Gold

BABCOCK & WILCOX
Lynchburg Research Center
P.O. Box 11165
Lynchburg, VA 24506
H. Moeller

BATTELLE-COLUMBUS LABORATORIES
505 King Avenue
Columbus, OH 43201
V. K. Sethi
I. G. Wright

BRITISH COAL CORPORATION
Coal Research Establishment
Stoke Orchard, Cheltenham
Glochester, England GL52 4RZ
M. Arnold
C. Bower
A. Twigg

BRITISH GAS CORPORATION
Westfield Development Centre
Cardenden, Fife
Scotland KY5OHP
J. E. Scott

BROOKHAVEN NATIONAL LABORATORY
Department of Applied Science
Upton, Long Island, NY 11973
T. E. O'Hare

CANADA CENTER FOR MINERAL & ENERGY TECHNOLOGY
568 Booth Street
Ottawa, Ontario
Canada K1A OG1
R. Winston Revie
Mahi Sahoo

CASE WESTERN RESERVE UNIVERSITY
Department of Metallurgy & Materials Science
516 White Bldg., 10900 Euclid Avenue
Cleveland, OH 44106
K. M. Vedula

COMBUSTION ENGINEERING
911 W. Main Street
Chattanooga, TN 37402
D. A. Canonico

CONSOLIDATION COAL COMPANY
4000 Brownsville Road
Library, PA 15129
S. Harding

ELECTRIC POWER RESEARCH INSTITUTE
P.O. Box 10412
3412 Hillview Avenue
Palo Alto, CA 94303
W. T. Bakker
R. L. S. Chang
J. T. Stringer
R. H. Wolk

EUROPEAN COMMUNITIES JOINT RESEARCH CENTRE
Petten Establishment
P.O. Box 2
1755 ZG Petten
The Netherlands
M. Van de Voorde

FOSTER WHEELER DEVELOPMENT CORPORATION
Materials Technology Department
John Blizard Research Center
12 Peach Tree Hill Road
Livingston, NJ 07039
J. L. Blough

GAS RESEARCH INSTITUTE
8600 West Bryn Mawr Avenue
Chicago, IL 60631
H. S. Meyer

GENERAL ELECTRIC COMPANY
1 River Road, Bldg. 55, Room 115
Schenectady, NY 12345
R. W. Haskell

IDAHO NATIONAL ENGINEERING LABORATORY
P. O. Box 1625
Idaho Falls, ID 83415
D. W. Keefer

LAWRENCE BERKELEY LABORATORY
University of California
Berkeley, CA 94720
A. V. Levy

LAWRENCE LIVERMORE LABORATORY
P.O. Box 808, L-325
Livermore, CA 94550
W. A. Steele

MOBIL RESEARCH & DEVELOPMENT CORPORATION
P. O. Box 1026
Princeton, NJ 08540
R. C. Searles

NATIONAL INSTITUTE OF STANDARDS AND TECHNOLOGY
Materials Building
Gaithersburg, MD 20899
S. J. Dapkunas

NATIONAL MATERIALS ADVISORY BOARD
National Research Council
2101 Constitution Avenue
Washington, DC 20418
K. M. Zwilsky

NEW ENERGY DEVELOPMENT ORGANIZATION
Sunshine 60 Bldg.
P.O. Box 1151
1-1, Higashi-Ikebukuro 3-chrome
Toshima-Ku, Tokyo, 170
Japan
S. Ueda

OAK RIDGE NATIONAL LABORATORY
P.O. Box 2008
Oak Ridge, TN
P. T. Carlson
J. H. DeVan
R. R. Judkins
J. L. Langford (8 copies)

RISOE NATIONAL LABORATORY
P.O. Box 49
DK-4000
Roskilde, Denmark
Aksel Olsen

SHELL DEVELOPMENT COMPANY
P. O. Box 1380
Houston, TX 77251-1380
L. W. R. Dicks

SOUTHWEST RESEARCH INSTITUTE
6620 Culebra Road
P.O. Drawer 28510
San Antonio, TX 78284
F. F. Lyle, Jr.

TENNESSEE VALLEY AUTHORITY
Energy Demonstration & Technology
MR 2N58A
Chattanooga, TN 37402-2801
C. M. Huang

TENNESSEE VALLEY AUTHORITY
1101 Market Street
MR 3N57A
Chattanooga, TN 37402
R. Q. Vincent

TEXAS EASTERN TRANSMISSION CORPORATION
P.O. Box 2521
Houston, TX 77252
D. H. France

THE MATERIALS PROPERTIES COUNCIL, INC.
United Engineering Center
345 E. Forty-Seventh Street
New York, NY 10017
M. Prager

THE TORRINGTON COMPANY
Advanced Technology Center
59 Field Street
Torrington, CT 06790
W. J. Chmura

UNIVERSAL ENERGY SYSTEMS, INC.
4401 Dayton-Zenia Road
Dayton, OH 45432
V. Srinivasan

UNIVERSITY OF TENNESSEE AT KNOXVILLE
Materials Science and Engineering
Department
Knoxville, TN 37996
C. D. Lundin

UNIVERSITY OF TENNESSEE SPACE
INSTITUTE
Tullahoma, TN 37388
J. W. Muehlhauser

WESTINGHOUSE ELECTRIC CORPORATION
Research and Development Center
1310 Beulah Road
Pittsburgh, PA 15235
S. C. Singhal

WESTINGHOUSE HANFORD COMPANY
P.O. Box 1970, W/A-65
Richland, WA 99352
R. N. Johnson

DOE
OAK RIDGE OPERATIONS OFFICE
P. O. Box 2001
Oak Ridge, TN 37831
Assistant Manager for Energy Research and
Development

DOE
OAK RIDGE OPERATIONS OFFICE
P. O. Box 2008
Building 4500N
Oak Ridge, TN 37831-6269
E. E. Hoffman

DOE
OFFICE OF BASIC ENERGY SCIENCES
Materials Sciences Division
ER-131, GTN
Washington, DC 20545
J. B. Darby

DOE
OFFICE OF CONSERVATION AND
RENEWABLE ENERGY
Energy Conversion and Utilization
Technologies Division
CE-12, Forrestal Building
Washington, DC 20545
J. J. Eberhardt

DOE
OFFICE OF FOSSIL ENERGY
Washington, DC 20545
D. J. Beecy (FE-14)
J. P. Carr (FE-14)
F. M. Glaser (FE-14)
T. B. Simpson (FE-25)

DOE
MORGANTOWN ENERGY TECHNOLOGY
CENTER
P.O. Box 880
Morgantown, WV 26505
R. A. Bajura
R. C. Bedick
F. W. Crouse, Jr.
N. T. Holcombe
W. J. Huber
J. E. Notestein
J. S. Wilson

DOE
PITTSBURGH ENERGY TECHNOLOGY
CENTER
P.O. Box 10940
Pittsburgh, PA 15236
S. Akhtar
T. C. Rupel
R. Santore
T. M. Torkos